Analysis of Three-Phase AC-DC Current Injection Hybrid Resonant Converter

R. Baharom, M. N. Seroji, M. K. M. Salleh, K. S. Muhammad
Faculty of Electrical Engineering, Universiti Teknologi MARA, Shah Alam, Selangor, Malaysia
rahimi6579@gmail.com

***Abstract*—This paper presents the analysis of high power factor three-phase AC-DC current injection hybrid resonant converter. The series-parallel (hybrid) configuration of the resonant converter using current injection technique is the key concept of this paper, which is realized by injecting the high-frequency resonant current to the diode-bridge rectifier. Featuring a high-power factor operation, the circuit offers low total harmonics distortion (THD) level of the input current waveforms, hence increase the quality of the power supply system. The analysis of the proposed converter is first carried out using MATLAB to investigate the feasibility and the effectiveness of the theoretical analysis. A prototype of a 1kW three-phase AC-DC current injection hybrid resonant converter (CIHRC) is then developed to support the simulation analysis. Selected simulation and experimental results are presented to verify the feasibility and the effectiveness of the theoretical analysis of the proposed converter.**

***Index Terms*—Three-Phase AC-DC Converter; Hybrid Configuration Resonant Converter; Current Injection Technique.**

I. INTRODUCTION

The circuit topology of three-phase AC-DC current injection technique based on the resonant converter was developed by the University of Birmingham in 2003 called the Current Injection Series Resonant Converter (CISRC) which started with a series circuit configuration [1]. The topology involved injecting the high-frequency currents into a three-phase bridge rectifier resulting in high-frequency modulation of the input rectifier voltage. The supply current was continuous, sinusoidal and in-phase with the supply voltage waveforms contributing to a high power factor and requiring only two MOSFET devices [1].

Subsequently, further works on small signal analysis and closed loop control of AC-DC three-phase current injection series resonant converter have been reported in [2] to improve the transient characteristics and to control or regulate the output voltage. Other works have shown that it was possible to remove the autotransformer with the inclusion of a straightforward high-frequency transformer by utilizing the full-bridge configuration of the current injection series resonant converter, which reduced the weight of the converter [3] [4].

Unfortunately, there has been no experimental verification reported for the circuit topology. Secondly, the use of series circuit configuration has a limitation to regulate the output voltage at a light or zero load conditions. This was due to the load current for series circuit configuration that varied in proportion to the resonant current.

To be in line with the availability of power electronics as an enabling technology, any development to provide an alternative topology for the CISRC results with the solution to eliminate their drawbacks whilst offering performance enhancement would be highly desirable.

The main objective of this paper is to extend the steady-state analysis of the three-phase AC-DC CIHRC as discussed in [5] by providing an experimental verification for the proposed circuit topology.

II. ANALYSIS OF THE THREE-PHASE AC-DC CIHRC

The three-phase AC-DC CIHRC as presented in [5] is shown Figure 1. The steady-state analysis of the approach circuit topology is assumed to have; a balanced and sinusoidal three-phase AC source, a linear line inductors without considering their saturation, and the three-phase diode bridge have infinite resistance during turn-OFF and zero resistance during turn-ON. It is also assumed that during at any given time, only one switch in each of the three legs of the converter can be turned-ON.

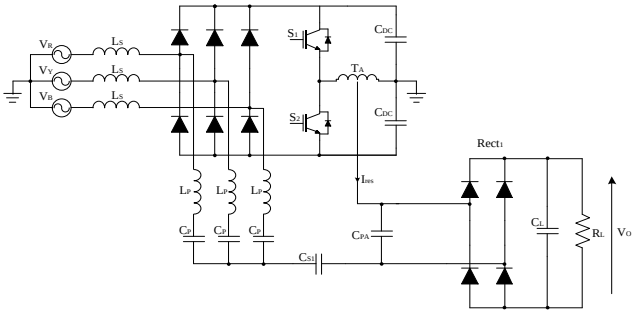

Figure 1: The three-phase AC-DC CIHRC

Figure 2(a) shows a single leg of converter fed by the hybrid resonant converter, whilst Figure 2(b) shows the fundamental frequency-equivalent circuit for the half-bridge hybrid resonant converter. V_S represents one of the phase voltages supplied by wye connected configuration. The resonant current I_{res3} is also considered as one-third of the converter resonant current I_{res} and is injected into the mid-point of the diode leg. The resulting modulation of the diode midpoint voltage V_{PWM} is modulated by a process of summation of the sinusoidal supply current I_{line} and the resonant current I_{res3}. When the sum of the two currents is greater than zero, the upper diode conducts and V_{PWM} is equals to $+V_{DC}/2$. Otherwise, the lower diode conducts when it less than zero and V_{PWM} becomes $-V_{DC}/2$.

The steady-state analysis could be derived based on the fundamental frequency equivalent circuit to determine the parameters of the proposed converter. The total impedance of Z_T is defined as the equivalent parallel connection of the

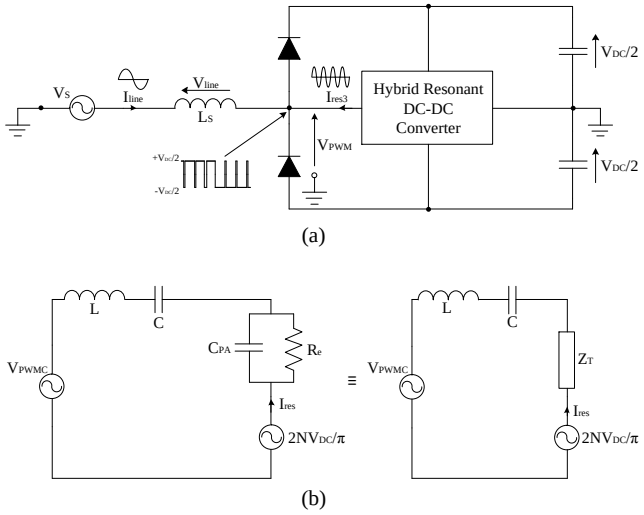

Figure 2: (a) Single leg of converter fed by hybrid resonant converter, (b) Fundamental frequency equivalent circuit for the half-bridge hybrid resonant converter

Steigerwald equivalent input resistance $R_e=\pi^2R/8$, with the capacitor C_{PA} which is the main different with the series circuit configuration. Based on [4], the modulation index M is defined as:

$$M = \frac{I_{line}}{I_{res3}} = \frac{3I_{line}}{I_{res}} \tag{1}$$

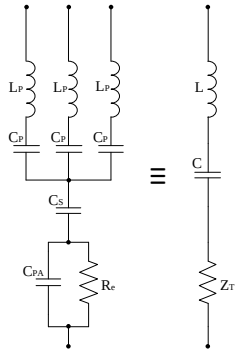

Figure 3: Equivalent resonant circuit topologies for zero-sequence harmonics

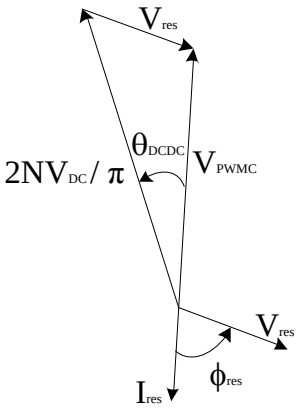

Figure 4: Phasor diagram for the zero-sequence resonant circuit, showing switching frequency components

Based on the assumption that the converter losses are zero, therefore the active input power would equal to the output power during the steady-state condition.

$$P_{in} = P_{out} \tag{2}$$

$$3\left(\frac{V_s}{\sqrt{2}}\right)\left(\frac{I_{line}}{\sqrt{2}}\right)\cos\phi_1 = \left(\frac{I_{res}}{\sqrt{2}}\right)Z_T = \frac{2}{\pi}I_{res}V_o \tag{3}$$

where;

$$Z_T = \frac{R_e}{1+\left(R_e\omega C_{PA}\right)^2}$$

As shown in Figure 3, by considering only the real output power, hence the equation (3) becomes:

$$3\left(\frac{V_s}{\sqrt{2}}\right)\left(\frac{I_{line}}{\sqrt{2}}\right)\cos\phi_1 = \left(\frac{I_{res}}{\sqrt{2}}\right)R_T = \frac{2}{\pi}I_{res}V_o$$

where, ϕ_1 is the displacement angle between the supply voltage V_s and line current I_{line}.

Substitute Equation (1), into Equation (3), hence;

$$I_{res} = \frac{MV_s}{Z_T}\cos\phi_1 \tag{4}$$

From the phasor diagram as shown in Figure 4, the switching leg voltage and current angle, θ_{DCDC} can be derived as;

$$\cos\theta_{DCDC} = \frac{{V_{PWMC}}^2 + \left(\frac{2NV_{DC}}{\pi}\right)^2 - {V_{res}}^2}{2V_{PWMC}\left(\frac{2NV_{DC}}{\pi}\right)} \tag{5}$$

Based on Figure 2(a), the mathematical terms can be derived as ;

$$\left(\frac{I_{res}}{\sqrt{2}}\right)^2 Z_T = \left(\frac{2NV_{DC}}{\pi\sqrt{2}}\right)\left(\frac{I_{res}}{\sqrt{2}}\right)\cos\theta_{DCDC} - \left(\frac{V_{PWMC}}{\sqrt{2}}\right)\left(\frac{I_{res}}{\sqrt{2}}\right) \tag{6}$$

Equation (5) can be used to eliminate $\cos\theta_{DC\text{-}DC}$ from Equation (6), and using (4) to eliminate I_{res}. Also noting that for the resonant circuit;

$$V_{res}\cos(\phi_{res}) = I_{res}Z_T \tag{7}$$

Hence, Equation (6) becomes:

$$\frac{{V_{PWMC}}^2}{V_s^2} - \left(\frac{2NV_{DC}}{\pi V_s}\right)^2 + \frac{2MV_{PWMC}\cos\phi_1}{V_s} + \left(\frac{M\cos\phi_1}{\cos(\phi_{res})}\right)^2 = 0 \tag{8}$$

The numerical method is used in order to solve Equation (8). Hence, the carrier harmonic voltage V_{PWMC} may be expressed as:

$$V_{PWMC} = \frac{V_{DC}}{2}f_c(M) \tag{9}$$

An approximate value of function f_c could be obtained from Figure 4 by utilizing a sixth order polynomial using MATLAB least squares function Polyfit over the interval M = 0 to 6, resulting in:

$$f_c(M) = 1.3017 - 0.6747M + 3.0386M^2 - 5.8822M^3 + 3.9844M^4 - 1.0205M^5 + 0.0650M^6 \quad (10)$$

Therefore, V_{PWM1} is expressed as:

$$V_{PWM1} = \frac{V_{DC}}{2} f_f(M) \quad (11)$$

Again, an approximate value of function f_f also could be obtained from Figure 4 using a sixth order polynomial, resulting in:

$$f_f(M) = -0.0295 + 1.3535M - 3.7018M^2 + 6.9740M^3 - 5.3M^4 + 1.6951M^5 - 0.1858M^6 \quad (12)$$

Then, based on Equation (11),

$$\cos\phi_1 = \frac{V_{PWM1}}{V_s} = \frac{V_{DC} f_f(M)}{2V_s} \quad (13)$$

Equation (9) and (13) can be substituted into equation (8) to give:

$$f_c(M) + 2Mf_c(M) f_f(M) + \left(\frac{Mf_f(M)}{\cos(\phi_{res})}\right) - \left(\frac{4N}{\pi}\right)^2 = 0 \quad (14)$$

By using Equation (10) and (12), Equation (14) can be solved numerically for M, using MATLAB's Fzero nonlinear zero finding algorithm.

$$\tan(\phi_{res}) = Q\left(\omega_n - \frac{1}{\omega_n}\right) \quad (15)$$

By using the values of modulation index M, obtained from Equation (14), the input displacement power factor $\cos\phi_1$ is calculated based on Equation (16).

$$\cos(\phi_1) = \frac{1}{\sqrt{1+\tan^2(\phi_1)}} = \frac{1}{\sqrt{1+\left(\frac{k_r M^2}{3}\right)^2}} \quad (16)$$

Where,

$$k_r = \frac{X_L}{Z_T}$$

The phase angle θ_{DCDC}, can be derived from Equation (6), using Equation (9) and (11),

$$\cos\theta_{DCDC} = \frac{\pi}{4N}\left(f_c(M) + Mf_f(M)\right) \quad (17)$$

III. EXPERIMENTAL SET-UP

This section introduces the construction of an experimental test-rig used to verify the proposed high power factor three-phase AC-DC current injection hybrid resonant converter. The hardware design was outlined completely with the power circuits, gate drives and its pulse width modulation (PWM) control circuits. A laboratory model of a three-phase AC-DC CIHRC was constructed and tested to compare the performance of the proposed converter with those implemented using computer models as described in the preceding section. The construction and component design of the experimental test-rig for three-phase AC-DC CIHRC consists of a three-phase diode bridge, power switches, DC link capacitor, a resonant tank, output full-bridge rectifier and line inductor.

The three-phase diode bridge was built with a three-phase rectifier bridge with fast recovery epitaxial diodes (FRED) types VUE 35-06NO7. With the voltage rating of 600 V, the current rating of 56 A and the reverse recovery time t_{rr} of 35 ns, was suitable for the high switching frequency operation of the converter. A heatsink was used to dissipate heat from the device in order to reduce power losses due to the heating effect.

In order to construct an inverter leg, two MOSFET device types coolMOS™ Power Transistor SPW47N60C3 were used and connected in a series configuration. This device consisted of voltage rating of 650 V, *ON* state resistance $R_{DS(on)}$ of 0.07 and a continuous drain current of 30 A and 40 A at the temperature T_c=100°C and T_c=25°C respectively. Similar to the three-phase diode bridge, each MOSFETs was also mounted onto a heatsink.

The power MOSFET devices were equipped with a gate drive that provided overcurrent protection as well as increasing the signal obtained from the PWM control circuit to an appropriate level before it was being fed into the power switching device. Since two power MOSFET were used in this work, an International Rectifier IR2110 gate drive circuit was used to drive the MOSFETs. The gate drive circuit consisted of a high side which was connected to the MOSFET 1 (M1) and a low side driver connected to the MOSFET 2 (M2). In order to essentially immune the gate drive circuit from any form of upset except direct overvoltage or over-dissipation, high-speed high current buffer/drivers capable of driving large MOSFETs, TC4422 were used. On the other hand, a resistor of 7.3 Ω was connected in a series with the gate terminal of the MOSFETs devices which was to damp any oscillation in the gate voltage and to ensure the dynamic current sharing. In addition, a 15 V 0.4 W zener diode was used to protect the MOSFETs gate by connecting the gate and source terminals.

In order to provide overcurrent protection to the MOSFETs devices, a CSNR151 Honeywell current transducer was connected in series with the lower MOSFET device to sense the current flow through the switching leg. Then, the output current transducer was connected to the high-speed differential comparator LM360 in order to compare the sensed current with the maximum current limit. A *D*-type positive edge-triggered flip-flop 74F74 was used to disable the IR2110 gate drive signal when the sensed current was over the maximum current limit.

The DC link capacitor used Metallized Polypropylene Film Capacitors (MKP) of 100 µF with 300 V voltage rating for

the individual split DC link capacitors as discussed in the previous section, the total DC link capacitor C_{DC} was 50 µF.

For the output full bridge rectifier implementation, two IXYS semiconductor-DSS2X101-015A Schottky Diode connected in series were used. A heatsink was used in order to compensate any switching losses which were not considered.

The prototype of the proposed converter fed with the three-phase variac used to gradually control the voltage at startup to the input line voltage up to 40 V_{rms}, 50 Hz. In addition, the isolating delta-star connection that was the interface between the converter and three-phase variac was used for safety.

IV. Results and Discussion

Figure 5 and 6 show the converter's output voltage, V_o and V_{DC} plotted against ω_n for N=1.4, Q=5 and k_r =0.198. It is seen from Figs. 5 and 6 that the experimental result agreed with the analysis and mathematical equations (prediction) and MATLAB simulation result, which showed the validity of the analysis and mathematical expressions in [5]. Figure 7 shows the red-phase input voltage and current waveforms. Using CIHRC technique, the pulsating supply current waveform becomes sinusoidal and almost in-phase with the input voltage waveform, thus, resulting in high power factor and low THD level. Table 1 tabulates the individual harmonic spectrums for the supply current waveform that was compared with the IEEE Std. 519. It can be seen that the harmonics spectrums of the supply current are well below than the acceptable limit that was defined by the standard. Figures 8 and 9 show the resonant current lag the voltage leg waveform and the output voltage with the supply voltage waveforms respectively.

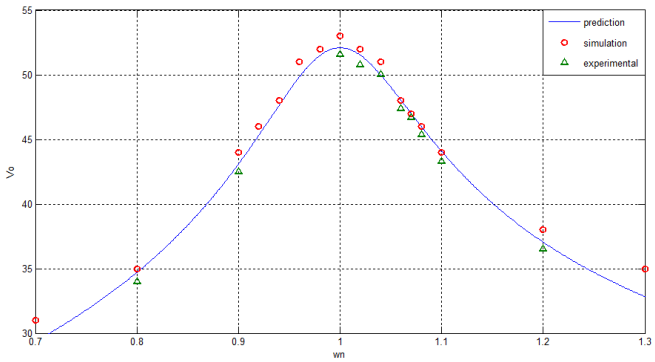

Figure 5: Converter output voltage plotted against ω_n for prediction, simulation and experimental test rig

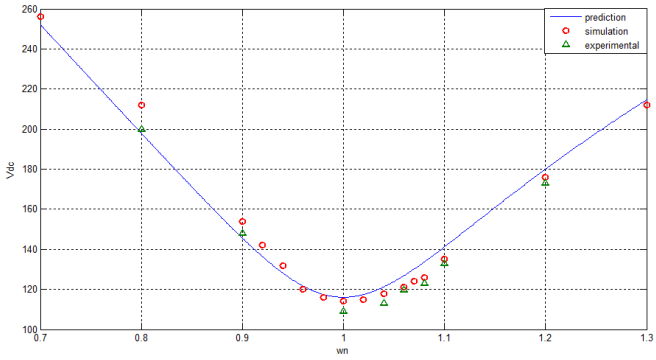

Figure 6: DC link voltage plotted against ω_n for prediction, simulation and experimental test

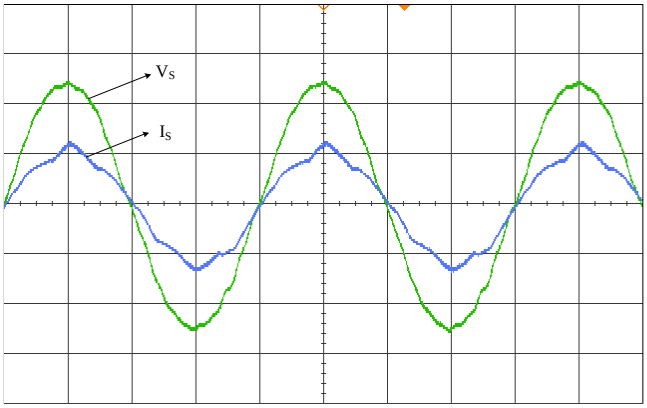

Figure 7: Red phase supply voltage (25 V/div, 5 ms/div) and current waveform (10 A/div, 5 ms/div)

Table 1
IEEE Std. 519 Standard Limits, Harmonics of Red Phase Supply Current, Power Factor (Pf) and Total Harmonics Distortion (THD) for the Experimental Results

Harmonics order	IEEE Std. 519 (%)	Simulation (%)
5th	4	2.62
7th	4	3.1
9th	4	0.29
11th	2	0.26
13th	2	0.69
15th	2	0.17
THD (%)		6.15
PF		0.985

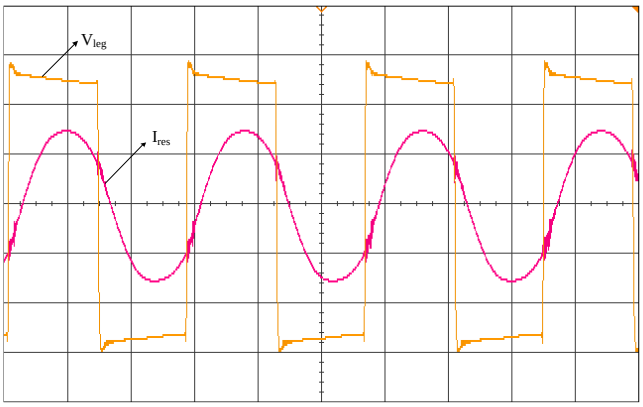

Figure 8: Converter resonant current (20 A/div, 16 µs/div) and switching leg voltage (22 V/div, 16 µs/div) for experimental results

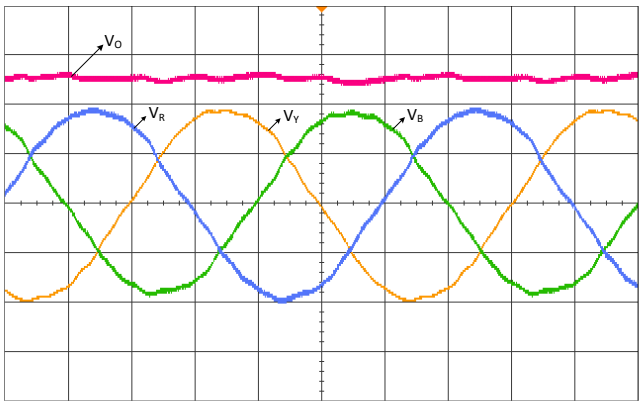

Figure 9: Converter output voltage (18 V/div, 3.3 ms/div) and supply voltages (30 V/div, 3.3 ms/div) waveforms

V. CONCLUSION

In this paper, detailed descriptions of the steady-state analysis and characteristics of the proposed three-phase AC-DC CIHRC were presented. Apart from the steady-state analysis, the experimental test-rig of the proposed work was also discussed. The proposed converter has been analysed and the performance of the converter validated through experimental results. The performance of the converter has been evaluated by assessing the total harmonic distortion (THD). The comparison of the individual harmonic spectrum of the red phase supply current waveform with the IEEE Std 519 showed that all of the harmonic spectrum were well below the acceptable limit and satisfied the standard. However, the THD level of the experimental test rig was slightly higher than THD obtained from the circuit simulation as discussed in [8]. These discrepancies were due to the prediction parameters based on a few assumptions:

- The utility is a three-phase balanced, sinusoidal voltage source.
- The line inductors are linear; saturation is not considered.
- Each of the six diodes was assumed to have infinite resistance when they are *OFF* and zero resistance when they are *ON*. At any given time, only one switch in each of the three legs of the converter can be turn-*ON*.
- The resonant current waveform is sinusoidal.

ACKNOWLEDGMENT

Financial support from Ministry of Higher Education Malaysia and Institute of Research Management and Innovation (IRMI) Universiti Teknologi MARA Grant No: 600-RMI/NRGS 5/3 (3/2013) is gratefully acknowledged.

REFERENCES

[1] Cross, A.M. ; Forsyth, A.J. "A high-power-factor, three-phase isolated AC-DC converter using high-frequency current injection", *Transactions on IEEE Power Electronics*, Volume: 18 , Issue: 4, Publication Year: 2003 , Page(s): 1012 – 1019.

[2] Seroji, M.N. ; Forsyth, A.J. "Small-Signal Model of a High-Power-Factor, Three-Phase AC-DC Converter with High-Frequency Resonant Current Injection", *International Conference on Power Electronics and Drives Systems, 2005. PEDS 2005*. Volume: 1, Publication Year: 2005, Page(s): 462 – 467.

[3] Omar, M.F. ; Seroji, M.N. ; Hamzah, M.K.; "Analysis and simulation of phase-shift control for three-phase AC/DC full-bridge current injection series resonant converter", *2012 IEEE Symposium on Industrial Electronics and Applications (ISIEA)*, Publication Year: 2012, Page(s): 114 – 117.

[4] Omar, M.F. ; Seroji, M.N. ; Hamzah, M.K.; " Analysis and simulation of three-phase AC/DC full-bridge current injection series resonant converter (FBCISRC)", 2010 IEEE Symposium on Industrial Electronics & Applications (ISIEA), Publication Year: 2010, Page(s): 159 – 164.

[5] Baharom, R.; Seroji, M.N.; Salleh, M.K.M., "Computer simulation model and performance analysis of high power factor three-phase AC-DC current injection hybrid resonant converter,"2015 IEEE 10th Conference on in Industrial Electronics and Applications (ICIEA), vol., no., pp.1403 1407, 15-17 June 2015